Title

Design Principles for Nanoparticles Enveloped by a Polymer-Tethered Lipid Membrane

Journal

ACS Nano, 9(10)

ISSN

1936-0851

Authors

Hu, Mingyang
Stanzione, Francesca
Sum, Amadeu K
et al.

Publication Date

2015-10-27

DOI

10.1021/acsnano.5b03439

Peer reviewed

Design Principles for Nanoparticles Enveloped by a Polymer-Tethered Lipid Membrane

Mingyang Hu,[†] Francesca Stanzione,[‡] Amadeu K. Sum,[‡] Roland Faller,[¶] and Markus Deserno[*,†]

Department of Physics, Carnegie Mellon University, Pittsburgh, Pennsylvania, USA, Department of Chemical and Biological Engineering, Colorado School of Mines, Golden, CO, USA, and Department of Chemical Engineering and Materials Science, UC Davis, CA, USA

E-mail: deserno@andrew.cmu.edu

Abstract

We propose the design for a nanoparticle carrier that combines three existing motifs into a single construct: a liposome is stabilized by anchoring it to an enclosed solid core via extended polymeric tethers that are chemically grafted to the core and physisorb into the surrounding lipid membrane. Such a design would exhibit several enticing properties, among them: (*i*) the anchoring stabilizes the liposome against a variety of external stresses, while preserving an aqueous compartment between core and membrane; (*ii*) the interplay of design parameters such as polymer length or grafting density enforces strong constraints on nanoparticle size and hence ensures a high degree of uniformity; and (*iii*) the physical and chemical characteristics of the individual constituents equip the construct with numerous functionalities that can be exploited in many ways. However, navigating the large parameter space requires a sound prior understanding for how various design features work together, and how this impacts potential pathways for synthesizing and assembling these nanoparticles. In this paper we examine these connections in detail, using both soft matter theory and computer simulations at all levels of resolution. We thereby derive strong constraints on the experimentally relevant parameter space, and also propose potential equilibrium and non-equilibrium pathways for nanoparticle assembly.

Introduction

One branch of nanotechnology that has seen impressive advances in the recent past is the design of sophisticated carriers for medical drugs.[1–7] The most common form of delivery vehicles—artificially designed nanoparticles (NP) with sizes up to a few hundred nanometer—exhibit many competitive advantages over the free drug, *e.g.* increased bioavailability of hydrophobic drugs,[8] prolonged half-life due to extra steric interactions from grafted polymers,[9,10] and an improved therapeutic index and lowered biotoxicity by targeted delivery.[2,11–14]

Along with the vigorous pursuit of concepts such as targeted delivery and controlled release, synthesis of nanoparticles with novel structures has always benefitted nanotechnology as a whole.[5] Liposomes and polymer-drug conjugates were used as the first generation of NPs and laid the foundation for the field of nanoscale drug delivery.[11] Several nanoscale therapeutics have been approved by the US Food and Drug Administration (FDA) since the 1995 approval of Doxil® (the anti-cancer drug doxorubicin encapsulated in PEGylated lipo-

*To whom correspondence should be addressed

[†]Department of Physics, Carnegie Mellon University, Pittsburgh, Pennsylvania, USA

[‡]Department of Chemical and Biological Engineering, Colorado School of Mines, Golden, CO, USA

[¶]Department of Chemical Engineering and Materials Science, UC Davis, CA, USA

somes).[15] Following the rapid takeoff of nanotechnology, increasing numbers of nanoparticles with potential applications in drug delivery or cancer diagnostics have been explored, including polymeric micelles, dendrimers, quantum dots, silica NPs, and carbon nanotubes, to name but a few.[5,7,12,16]

Despite significant progress in the field, some basic limitations of the aforementioned constructs persist. For instance, with most of the drug delivery systems, even after the employment of the additional "targeting" strategies (no matter whether passive or active), the accumulations of the drug in the tumor cells is normally less than 10%: most of the drug-loaded NPs end up in the liver and spleen, and a non-negligible fraction may get destabilized during circulation.[13,17] These troubles are compounded by the fact that accumulation at the right place does not guarantee *uptake*: prior to arriving at their target location, a sizable fraction of NPs might have lost part or all of their payload during circulation,[13,17] while others may experience difficulties entering the cells due to suboptimal size and/or shape.[18,19]

There are two ways to address these issues: refine existing constructs and envision new designs. Mudshinge *et al.* argue that a technology platform that enables versatile control over NP size, shape, and surface chemistry is a critical first step for both developing appropriate tools and gaining a deeper scientific understanding of nanoparticles.[5] Moreover, computer simulations can guide the optimization of any new design, complementing experimental insight into the mesoscopic underpinnings of its function.[6] With this motivation, we here propose a novel NP design for drug delivery, whose structure can be found in Fig. 1, and provide an extensive analysis of its underlying physical design constraints. In this nano-composite, a liposomal vesicle is tethered with amphiphilic linker molecules to a solid spherical core. Each linker contains a headgroup that covalently binds to the core, a hydrophilic polymer spacer of adjustable length and low dispersity, and a lipid-like hydrophobic anchor that inserts into the lipid vesicle surrounding the entire construct. An example realization would be polyethylene glycol (PEG) grafted onto a gold nanoparticle through standard thiol chemistry, with a lipid moiety conjugated to the other end to anchor the polymer into the enclosing liposome.

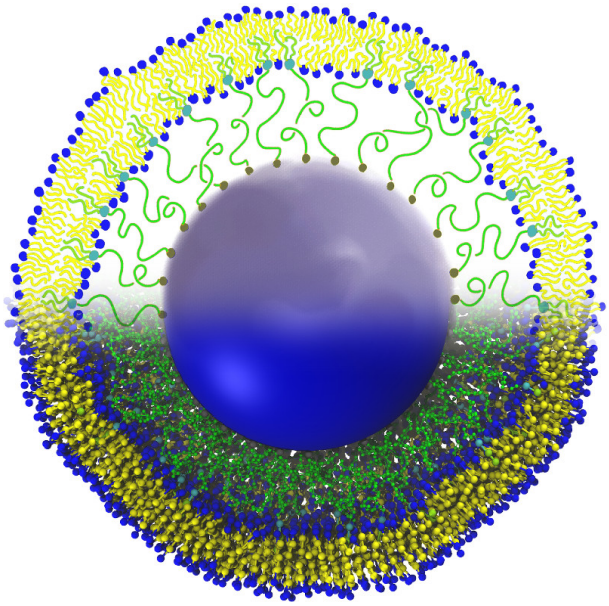

Figure 1: The proposed nano-composite structure. The upper half of the figure is a schematic, while the lower half is taken from a simulation snapshot. The blue sphere in the center is the NP core, to which polymers (green) are tethered that terminate in a lipid molecule (cyan head an green tail), which in turn anchor the enclosing bilayer of lipids (blue heads and yellow tails).

We will argue that by combining design principles that have individually proven successful in other nanoscale drug carriers, our proposed structure not only inherits beneficial properties from its components but acquires novel characteristics useful to its function. It therefore has the potential to make headway on at least the following three fronts:

1. The interplay between polymers and lipids enforces strong constraints on NP assembly. In particular, their size is largely defined by the free energy minimum dictated through key design parameters, such as grafting density or polymer contour length. Hence, one attains a fine control over NP size and dispersity through the choice of *components*, rather than the particulars of a *kinetic process*, and may thus reduce the impact of the production process or the extent of batch-to-batch variations. This matters because having NPs with a pre-defined narrow size dis-

tribution is paramount for their biodistribution,[18–20] the internalization into cells,[21–23] and even for the potential enhancement of apoptosis pathways.[24]

2. Tethering the lipid vesicle to a solid core suggests an enhanced stability against typical failure modes, compared to liposomal NPs, and this increases the NP's probability of arriving at the target intact. For instance, core and polymer cushion will bolster the membrane coat against both normal and shear stresses. And localized partial rupture events are counteracted not only by the polymers pulling lipid patches back, but also by the hydrophobic anchors providing stabilizing non-removable self-assembly nuclei that equip the lipid matrix with self-healing properties. It is indeed well documented that bilayer membranes sparsely tethered to (flat) substrates strongly gain in stability, with lifetimes approaching several months.[25]

3. The combination of a liposomal vesicle and a solid NP core offers the possibility of "theranostics" (a therapy/diagnosis hybrid),[26–28] with the lipid vesicle responsible for drug trafficking and the core (*e.g.* gold and iron oxide NPs are good candidates) doubling for additional diagnostic imaging purposes.[28,29]

Although this novel structure might seem complex and exotic at first glance, its design is based on several existing and well understood precursors: liposomes have been considered for drug delivery since 1965;[10,30,31] planar tethered bilayer membranes have become a key model systems to study membrane-protein interactions;[25,32–35] and core-shell-type lipid-polymer hybrid NPs have been devised as a delivery platform.[36] The motif of polymer decorated NPs in particular has a rich history into which our design can tap. Such constructs have been used for functionalized emulsion stabilization,[37,38] programmable NP assembly,[39–41] gene delivery,[42,43] DNA detection,[44,45] cancer targeting and imaging,[46,47] and many other applications. Moreover, the synthesis of very uniform polymer brushes on the surface of NPs can be achieved by atom transfer radical polymerization,[48,49] allowing an exquisite control of grafting density and hybrid particle size.

In gene therapy, the active ingredient is a polymer itself (single- or double-stranded nucleic acid). Using oligonucleotides as tethers in our NP constructs hence constitutes another conceivable functionalization, which is based on well-explored model systems. Indeed, Rosi *et al.* have synthesized oligonucleotide (ON) functionalized gold nanoparticles and shown that they exhibit a number of advantages over conventional transfection agents.[43] While these constructs are still ultimately degraded by nucleases, their data show that this happens about an order of magnitude slower than for free ONs, presumably because the arrangement of ONs on the nanoparticles leads to steric hindrances.[43] Coating this structure with a lipid bilayer anchored to suitably functionalized ends of the ONs could further enhance degradation resistance (at least against extracellular nucleases during delivery), besides providing additional opportunities for immunoprotection and targeting along the same lines employed for liposomes.[47,50,51]

In addition to being inspired by several existing systems, many of the strategies that have been proposed and/or shown to improve the performance of drug carrier vehicles can also be used with our design. Most notably, a host of surface decoration techniques aimed for instance to prolong circulation or targeting of liposomal carriers also apply in our case, since they are quite independent of whatever happens in the liposome's interior. And if the NP core is chosen as metallic, its photothermal properties can be exploited for both therapy and controlled release.[8] In the present work we are, however, more concerned with basic consequences of the core-polymer-membrane architecture, and so we will not discuss such biomedically exciting ramifications, as they are largely incidental for physical material properties such as structure and stability.

Meanwhile, the theoretical and computational methods we will use to approach the problem have also been applied throughout the history of drug delivery and oncology: mathematical modeling of drug release was already introduced into the field in the 1960s following the seminal works

by Higuchi;[52,53] physical factors have also drawn the attention of many researchers;[17,54] thanks to the rapid advances in computation ability, drug-delivery-related problems, such as the uptakes of NP into lipid membranes[55] and NP design,[56] have become tangible using computer simulations.

To the best of our knowledge, such NP structures have not yet been assembled in experiments. In fact, without any prior understanding how core size, polymer length and stiffness, tethering density, membrane rigidity, anchor insertion energy and several other parameters affect structure, stability, and function of the resulting product, one would have to scan through a very large parameter space in order to find a superior design. The aim of this paper is to provide this understanding by using well known principles from soft matter physics to discuss thermodynamic stability and potential kinetic pathways leading to polymer-membrane coated NPs.

Results

We will begin with a discussion of relevant generic considerations about this system from the perspectives of geometry and polymer theory. These will then be cross-checked against atomistic and coarse-grained (CG) molecular dynamic simulations, the latter at two different levels of resolution. In the end, further simulations suggest a potential process to assemble the proposed nanocomposites.

Theoretical considerations

In this subsection, generic considerations due to geometry and polymer chemistry will be introduced.

Grafting density

The average number of polymers anchored on the surface of the nanoparticle core per unit area is called the grafting density, Σ. The finite footprint a_{linker} of the endgroups adsorbed to the surface leads to an obvious upper limit for Σ: considering only the excluded volume interactions among the endgroups, this limit amount to

$$\Sigma \leq \Sigma_{\max} = 1/a_{\text{linker}}\,. \tag{1}$$

On the other hand, we assume Σ can be tuned *down* from this maximum value by placing "placeholders" or "backfillers" on the core surface, as used in the case of planar tethered bilayer membranes.[33,35,57] The local arrangement of these can normally not easily be controlled, which might lead to heterogeneities in grafting.

Depending on the assembly process, a *minimum* grafting density $\Sigma_{\min}$ may also arise. During assembly one needs to wrap a membrane into a curved shape enclosing the NP. If the ground state of the membrane is flat, then curving it will cost energy, which in turn could come from various sources, such as the line tension of open lipid patches which strive to close up.[58–60] However, if membranes are present as much larger structures (*e.g.* giant unilamellar vesicles), which are essentially flat in comparison to the NP's final curvature radius, then the only obvious term that can balance the bending energy is the free energy gained from inserting the lipid anchors into the membrane. The latter can be written as $E_{\text{ins}} = \varepsilon_{\text{ins}} 4\pi R_{\text{core}}^2 \Sigma$, where ε_{ins} is the free energy of insertion of a single anchor and R_{core} is the radius of the solid core. This needs to exceed the energy cost of bending the membrane into a sphere, $E_{\text{bend}} = 4\pi(2\kappa + \overline{\kappa})$, where κ and $\overline{\kappa}$ are the bending modulus and the Gaussian curvature modulus of the membrane, respectively.[58,61] Requiring that insertion must pay for bending leads to the lower bound

$$\Sigma \geq \Sigma_{\min}^{(1)} = \frac{2\kappa + \overline{\kappa}}{\varepsilon_{\text{ins}}} \frac{1}{R_{\text{core}}^2}\,. \tag{2}$$

When the membrane is stiff, or the free energy of insertion is low, or when the solid core is small, we need a larger grafting density.

A second lower bound on Σ stems from the experience with planar tethered bilayer membranes. In order to keep a planar tBLM firmly tethered to the substrate, the anchor-to-lipid ratio ϕ should not drop below about 10%.[35] Because of the spherical geometry, this constraint is translated in terms of grafting density on the core surface as

$$\Sigma \geq \Sigma_{\min}^{(2)} = \frac{\phi}{a_\ell} \left(\frac{R_{\text{ves}}}{R_{\text{core}}} \right)^2, \tag{3}$$

where a_ℓ is the area per lipid.

To stay on the safe side, one may take the

larger value from Eqs. 2 and 3 as the lower bound $\Sigma_{\min}$ for the grafting density: $\Sigma \geq \Sigma_{\min} = \max\{\Sigma^{(1)}_{\min}, \Sigma^{(2)}_{\min}\}$. Notice that (*i*) both constraints are optional if wrapping is not involved in the assembly process, and (*ii*) these two limits become identical when the total insertion free energy $E_{\rm ins}$ equals the bending energy $E_{\rm bend}$ of the vesicle.

Vesicle radius

Besides the restrictions on the polymer linkers alone, a more important aspect of our design is the interplay between the polymers and the enclosing membrane. Given a membrane of a *fixed* number of lipids, the polymers may push or pull on it. If they are too crowded in the space between the NP core and the surrounding bilayer, they exert an outward pressure on the membrane; if instead they can only span the distance between core and bilayer by being stretched beyond their equilibrium length, they create an inward pull, which one might formally view as a negative pressure. Clearly, such polymer-membrane interactions affect the possible range of the nanocomposite's size.

To semi-quantitatively predict the polymer-membrane interactions, we introduce a theoretical model for the polymer brush confined between two concentric spheres, mimicking the polymers in our nanocomposites. The force-extension relation of the brush derived from this model can then be employed to systematically optimize the system parameters.

A lower bound on the radius of the vesicle, $R_{\rm ves,min}$, exists due to the increasing (osmotic) pressure from the polymers when the vesicle size decreases. The pressure Π from the polymer brush induces a surface tension σ in the lipid membrane according to the Young-Laplace relation $\sigma(R_{\rm ves}) = \Pi(R_{\rm ves})R_{\rm ves}/2$. When σ exceeds the rupture tension $\sigma_{\rm rup}$ of the membrane, pores will form, accompanied by loss of drug payload.

This pressure Π can be semi-quantitatively predicted using a simple scaling theory originally due to de Gennes.[62,63] In the semi-dilute regime, where the Flory radius of the chains is smaller than the intermolecular distance, the pressure can be written as $\Pi \simeq k_{\rm B}T/\xi^3$, where $k_{\rm B}T$ is the thermal energy and ξ is the characteristic length scale of the polymer solution.[62] Adapting the results for planar tethered polymer brush[64,65] to the spherical case here, one derives the force-extension relation of the brush in the *strong compression* regime as[66]

$$\Pi(R_{\rm ves}) \approx \frac{k_{\rm B}T}{\xi_0^3}\left(\frac{\Phi(R_{\rm ves})}{\Phi_0}\right)^{9/4} \tag{4}$$

$$\approx \frac{k_{\rm B}T}{\xi_0^3}\left(\frac{R_0^3 - R_{\rm core}^3}{R_{\rm ves}^3 - R_{\rm core}^3}\right)^{9/4}, (R_{\rm ves} < R_0) \tag{5}$$

where Φ is the monomer volume fraction and the subscript '0' denotes the reference state when the polymers are relaxed: R_0 is the radius of the chain ends at which the linkers are relaxed, and $\xi_0 = (R_0/R_{\rm core})/\sqrt{\Sigma}$ is the average distance between two anchoring sites at $R = R_0$. A derivation of this result is given in the Supporting Information. When the vesicle size $R_{\rm ves}$ is reduced, the monomer fraction Φ and the pressure Π increases and the membrane tenses. The lower bound of the vesicle size is reached when the membrane reaches the rupture tension, leading to

$$\frac{1}{2}R_{\rm ves,min}\,\Pi(R_{\rm ves,min}) = \sigma_{\rm rup}\,. \tag{6}$$

There also exists an upper bound of the vesicle size, $R_{\rm ves,max}$. In large vesicles, the polymer chains are stretched beyond their relaxed length. These chains thus contract and deform the vesicle, before reaching a point when the vesicle is so large that the hydrophobic anchors are pulled out from the membrane. Since this happens when the chains are in the large extension regime, the interactions between the neighboring chains are negligible, and the behavior of the polymer brush can be approximated by single-chain theories.

If the persistence length $\ell_{\rm p}$ and contour length L_0 are known, the force-extension curve $F_{\rm stretch}(L)$ can be calculated. Since for the type of polymers we have in mind (such as PEG) the persistence length is not much bigger than the bond length $b = L_0/N$, we need to use a *discrete* version of the

worm-like chain:[67,68]

$$\frac{F_{\text{stretch}}(L)\,b}{k_{\text{B}}T} = \frac{1}{\tilde{b}}\left[\sqrt{1+\tilde{b}^2/(1-\xi)^2} - \sqrt{1+\tilde{b}^2}\right] + \left(3\frac{1-\mathcal{L}(1/2\tilde{b})}{1+\mathcal{L}(1/2\tilde{b})} - \frac{\tilde{b}}{\sqrt{1+\tilde{b}^2}}\right)\xi\,, \tag{7}$$

where $k_{\text{B}}T$ is the thermal energy, and $\xi = L/L_0$ is the end-to-end extension normalized by the contour length L_0, $\mathcal{L}(x) = \coth(x) - 1/x$ is the Langevin function, and $\tilde{b} = b/(2\ell_{\text{p}})$. This differs from the well known worm like chain (WLC) expression of Marko and Siggia,[69] especially in the high strain limit, where it diverges like $1/(1-\xi)$ instead of $1/(1-\xi)^2$, but in the continuum limit $b \to 0$ it again reduces to the standard WLC expression.

Stretching a polymer leads to the excess energy

$$E_{\text{stretch}}(L) = -\int_0^L \mathrm{d}L'\, F_{\text{stretch}}(L')\,, \tag{8}$$

which will result in anchors being pulled out of the membrane if the tensile energy in the polymer exceeds the free energy of anchor insertion into the bilayer, ε_{ins}. This leads to an upper bound for the vesicle radius,

$$E_{\text{stretch}}(R_{\text{ves,max}} - R_{\text{core}}) \leq \varepsilon_{\text{ins}}\,, \tag{9}$$

where typically $\varepsilon_{\text{ins}} \sim 20\,k_{\text{B}}T$.

The cross-over regime between stretching and compression is difficult to describe analytically. However, we will make the simple assumption that the force per chain simply arises as the sum of the two contributions calculated above. Since each contribution becomes small in the regime in which the other is large, this effectively produces a smooth interpolation between the two limits.

Molecular Dynamics simulations

In this section we will check the theory described so far using Molecular Dynamics simulations at various levels of resolution.

Atomistic simulations

On this most refined level it is unrealistic to study a complete NP complex. However, we can investigate *local* phenomena, in particular the critical aspect of anchor insertion into the bilayer. We have argued above that if the tethers are stretched too strongly, the entropic polymer tension will pull the anchoring group out of the bilayer it is supposed to tether. To test whether our theoretical framework captures the mechanics of this process, we conducted atomistic simulations of differently sized PEG tethers with a dioleoylglycerophosphatidylethanolamine (DOPE) anchoring group out of a dioleoylglycerophosphatidylcholine (DOPC) membrane. We also varied the width of the aqueous region between the solid substrate and the membrane.

We started with a tethering molecule having 29 PEG units, corresponding to a fully stretched length of 10.15 nm, and a width of 5.9 nm between the solid support and the surface of the DOPC membrane, of which 1.3 nm are taken up by the chemical group grafting the tether to the substrate. Under these conditions the tether is very stable and the anchor is soundly inserted into the membrane. Taking $b = 0.35\,\text{nm}$ and $\ell_{\text{p}} = 0.32\,\text{nm}$, Eqn. (7) predicts $F_{\text{stretch}} \approx 12.6\,\text{pN}$. This force is much too small to pull a chain out of the membrane, as the following semi-quantitative argument shows. The free energy of hydration of a simple hydrocarbon chain is about $0.884\,\text{kcal/mol}$ per CH_2 group.[70] A stretched hydrocarbon chain measures 0.125 nm per CH_2 unit, and we must extract two chains per lipid. However, the two chains are close, and so they mutually screen their apposing hydrophobic surfaces. While it is difficult to precisely calculate the extent of this effect, we can estimate its magnitude by a simple qualitative argument: picture the cross-section of a single chain as a square of side length a; upon extracting from the bilayer, each side gets exposed to water and hence contributes to the hydration free energy. If we extract two neighboring tails, this corresponds to two *touching* squares with a joint circumference of $6a$, not the individual $2 \times 4a$, and this suggests an estimated reduction factor of $3/4$ due to screening. Taking everything together, we therefore arrive at the fol-

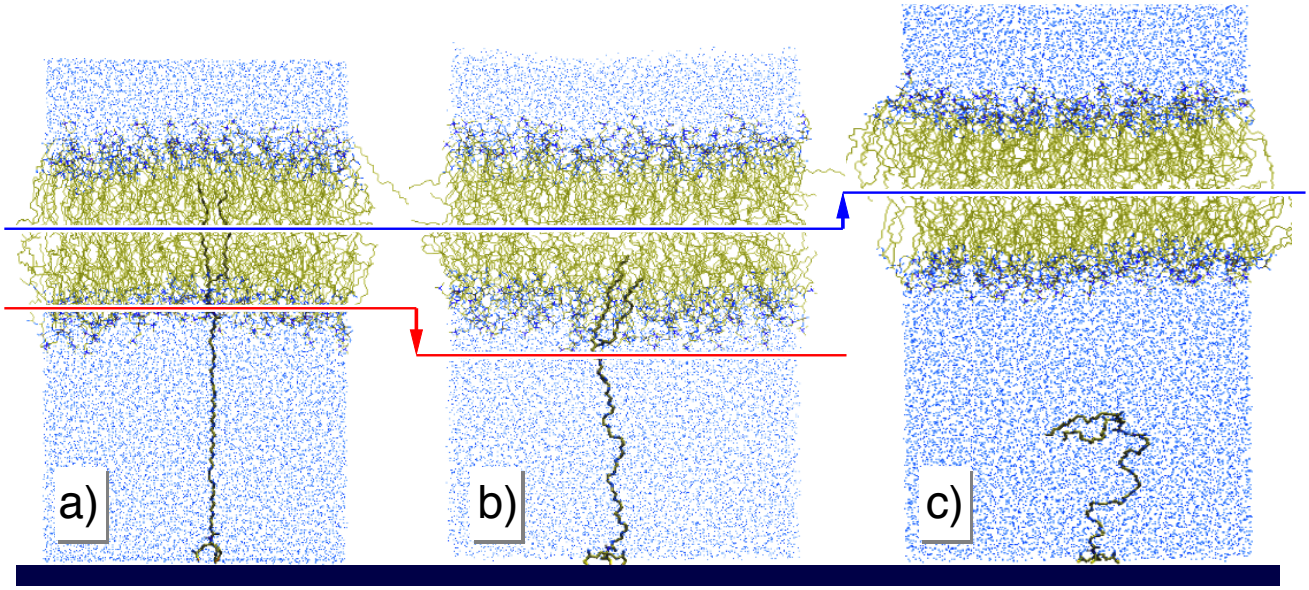

Figure 2: Pull-out of a PEG-tethered lipid (14 PEG units) from a DOPC membrane. In all panels bilayer lipids are shown with yellow tails and dark blue head groups. Water molecules are light blue. The PEG tether and its terminating lipid (protruding into the bilayer in panels a and b) is indicated with thicker lines and darker hues. a) Initial starting configuration with a membrane separated 5.9 nm away from the substrate; b) after 100 ns the tether is partially pulled out of the membrane; c) if the membrane is separated an additional 0.83 nm away from the substrate, the entropic tension in the tether suffices to completely extract the lipid.

lowing estimate for the extraction force:

$$F_{\text{extract}} \approx \frac{2 \times \frac{3}{4} \times 0.884\,\text{kcal/mol}}{0.125\,\text{nm}} \approx 74\,\text{pN}\,, \quad (10)$$

which is ~ 6 times bigger than the actual force with which the PEG-29 tether pulls on the lipid.

Reducing the number of PEG units, the tether is stretched and the tug on the anchor increases. When we reach 14 PEG units (see initial configuration in Fig. 2a), the total extended PEG chain length shrinks to 4.9 nm. Adding the 1.3 nm of the grafting group, the linker length is 6.2 nm, which is still bigger than the separation between membrane and substrate. Judging by *geometry*, one might expect the lipid to stay inserted, but the trouble is *energy*: the "slack" of only 0.3 nm is so small that the tensile force predicted by Eqn. (7) is now $F_{\text{stretch}} \approx 177\,\text{pN}$, much bigger than our estimated extraction force of 74 pN. However, the lipid is not yet fully pulled out of the membrane—see Fig. 2b. This happens because the pulling force decreases as the PEG chain contracts. Eqn. (7) shows that the tension in the PEG chain balances the estimated extraction force once the tether has contracted to about 85% of its fully extended length, about 4.16 nm. We hence expect the lipid to be pulled $5.9\,\text{nm} - (4.16\,\text{nm} + 1.3\,\text{nm}\,\text{nm}) = 0.44\,\text{nm}$ (or about 3.5 CH_2 units) out of the membrane. In reality, the lipid is pulled out a bit further (see again Fig. 2b), showing that the above reasoning is of course only semi-quantitatively correct. If we now increase the distance between the substrate and the membrane to 6.73 nm, adding an extra 0.83 nm, the balance condition would now hold when $0.44\,\text{nm} + 0.83\,\text{nm} = 1.27\,\text{nm}$ (or about 10 CH_2 units) are being pulled out. This is more than half the lipid tail length (DOPC has 18 carbons in each chain), and so the anchor is finally extracted completely from the bilayer, see Fig. 2c.

Coarse-grained simulations

To study the whole NP complex, we change to a strongly coarse-grained level. To ensure that we investigate a realistic scenario, we combine the theoretical constraints (especially the limits on vesicle size) to identify a possible range of stable NPs before the simulation is started. Of course, the goal is really to use such constraints as restrictions

on *experimental* parameters. The point of the CG simulations is therefore to test, whether the theoretical predictions capture the behavior of model NPs, and if yes, how well.

Let us therefore consider an example system to illustrate the theoretical considerations described above. This system consists of a solid spherical core of radius $R_{\rm core} = 9.0\,{\rm nm}$ and $f = 342$ linker chains, giving a grafting density $\Sigma \simeq 0.34\,{\rm nm}^{-2}$. Each chain contains $N = 30$ monomers of bond length $a = 0.40\,{\rm nm}$, and persistence length $\ell_{\rm p} \approx 0.32\,{\rm nm}$, mimicking commonly-available uniform soft polymers such as polyethelene-glycol (PEG). Assuming the enclosing vesicle is made of regular lipid membrane ($2\kappa + \overline{\kappa} \sim 20 k_{\rm B}T$) and the polymers are within their extension range ($r \leq R_{\rm core} + L_0$, where r is the radial position of the chain ends), the requirements on the grafting density, Eqs. (1), (2) and (3), are satisfied. Note that the vesicle radius $R_{\rm ves}$, defined by the radius of the membrane midplane, is related to the position of the chain ends r by $R_{\rm ves} = r + d/2$, where d is the membrane thickness. Moreover, the Flory radius of each chain $R_{\rm F} = aN^{3/5} \approx 2.2\,{\rm nm} > \xi = \sqrt{1/\Sigma} \approx 1.7\,{\rm nm}$, so we are in the semi-dilute regime, as assumed in the theory.

The predicted force-extension relation of the example system is shown as the red dashed curve in Fig. 3. As expected, the force diverges at large compression ($r \to R_{\rm core} = 9\,{\rm nm}$, when the pressure from the polymers could easily burst the membrane) and large extension ($r \to R_{\rm core} + L_0 \simeq 21.1\,{\rm nm}$, when the chains are fully stretched).

In order to test this prediction, a set of molecular dynamic (MD) simulations of the polymer chains were conducted, using a simulation model extended from a generic coarse-grained (CG) lipid model.[71,72] A schematic of the model can be found as an inset in Fig. 3. The phase behavior and elastic properties of the original membrane model have been well characterized,[60,73,74] and it has been successfully used to study phenomena such as curvature-mediated lipid sorting,[75] membrane poration by antimicrobial peptides,[76] membrane mediated interactions,[77] and supported bilayer membranes.[78] The polymer part of the tethers is modeled using a simple bead-spring model.[79] Details of the parameterization of this model are described in the Method section, as well as in the Supplementary Information.

In the simulations, one end of each chain was fixed at a radius $R_{\rm core}$ from the center of the core, while the other end was held at different radii r by a harmonic potential. A spherical impenetrable shell was also applied to confine the linker particles within the radius r to mimic the lipid vesicle. At each r, the average force to hold the chain ends and the force due to the pressure on the constraining shell were measured and then converted into the force per chain, $F(r)$, to compare with our theory. Shown as the solid dots in Figure 3, our theory semi-quantitatively predicts the forces throughout the full range of vesicle radius.

Vesicle size and stability

With the tested force-extension relation of the polymer brush, the next step is to check the aforementioned range of vesicle size. The lower bound of the vesicle radius $r_{\rm min} = 11.9\,{\rm nm}$ is predicted by Eq. (6), when the membrane bursts due to inner pressure. This value depends on the rupture tension of our membrane, $\sigma_{\rm rup} \sim 2.34\,\varepsilon/\sigma^2 \sim 14\,{\rm mN/m}$, which we determined using the pore-opening protocol discussed in Cooke and Deserno.[72] The upper bound for the radius follows from Eq. (9), and we find $r_{\rm max} = 17.6\,{\rm nm}$ as the radius at which chain anchors are starting to get pulled out, using a value for the pullout free energy per chain of $15 k_{\rm B}T$. These two bounds are shown as dotted vertical lines in Fig. 3.

Stable vesicle sizes should lie in the window $(r_{\rm min}, r_{\rm max})$. More importantly, if the nanocomposite is allowed to freely adjust the number of lipids in its membrane coat, then it is most likely to find vesicles with a tension-free polymer brush ($r = 13.2\,{\rm nm}$ in this case), when the total free energy of the system is minimized. (Recall that the curvature energy of a spherical vesicle does not depend on size.)

To validate this hypothesis, four complete NP simulations were conducted with different vesicle radii $R_{\rm ves}$. In all simulations, we started with a fixed solid core, the same polymer brush of 342 linkers discussed above, and a *pre-assembled* lipid vesicle of radius $R_{\rm ves}$. The number of lipids per leaflet was initially adjusted to account for the presence of anchors in the inner leaflet, but since

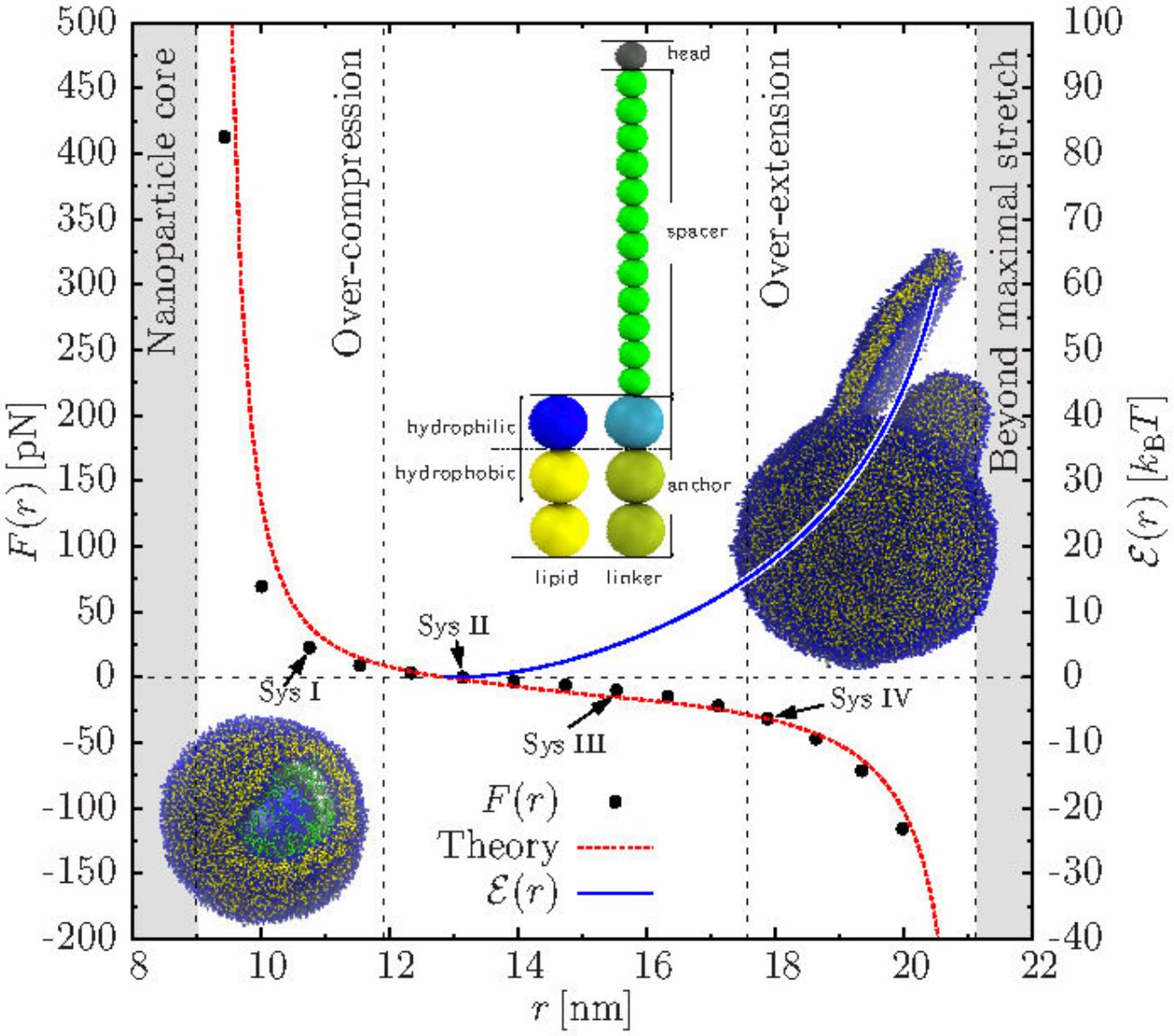

Figure 3: The force-extension curve for a single chain in the example system, as predicted by our theory (red dashed curve) and measured in MD simulations (solid dots, errors are smaller than the symbols). The horizontal axis $r = R_{\text{ves}} - d/2$ is the position of the chain ends, the vertical axis on the left labels the force per chain $F(r)$, and the vertical axis on the right is the free energy per chain, $E_{\text{stretch}}(r)$ (blue curve). Note that the repulsive (positive) force diverges at the core surface ($r = 9.0\,\text{nm}$, shaded), while the contractile force (negative) diverges when the chains are fully extended ($r = 21.1\,\text{nm}$, shaded). The predicted range of a physically viable vesicle size, *i.e.*. $r_{\text{min}} \simeq 11.9\,\text{nm}$ by Eq. (6) and $r_{\text{max}} \simeq 17.55\,\text{nm}$ by Eq. 9, is indicated by two vertical dotted lines. Two snapshots of an overly small vesicle (brush over-compressed) and an overly large vesicle (brush over-extended) show examples of how the polymers can destabilize and deform the enclosing membrane vesicle. A schematic of the CG model is also shown on the upper middle of the panel.

the Cooke model has a high rate of lipid flip-flop, any remaining imbalance of the lipid's chemical potential between the two leaflets is quickly relaxed. All anchors were initially placed inside the membrane, and they were found to still reside there at the end of the simulations of length $3 \times 10^4\,\tau$ (which maps to approximately $300\,\mu$s). Due to the different initial sizes, the four pre-assembled vesicles will try to enforce a polymer extension that corresponds to $r = 10.9\,$nm (System I in Figure 3, forming an over-compressed brush), 12.9 nm (System II, allowed), 15.4 nm (System III, allowed), and 17.8 nm (System IV, over-stretched). The number of lipids in the vesicles was determined from the known area per lipid of the model and the desired initial vesicle size.

For System I, the smallest vesicle, the polymer chains were too confined and thus exerted a large pressure on the vesicle; as expected, the membrane ruptured and a pore formed (bottom left inset in Fig. 3). Two other systems, II and III, which are within the "permitted" range of vesicle size, stayed stable and spherical throughout the entire simulation time of $3 \times 10^4\,\tau$ ($\sim 300\,\mu$s), as expected from our theoretical considerations. A typical snapshot for these two system resembles the one in Fig. 1.

In System IV the vesicle size exceeded the maximum allowed value predicted by our theory, but contrary to expectation the chain anchors did not pull out of the bilayer. Instead, the system responded by a *cooperative shedding of lipids* from the vesicle. The "negative pressure" induced by the tense polymer chains leads—again via Young-Laplace—to a lateral compression of the bilayer. For a free bilayer one would expect a shape change or buckling, but polymer anchoring largely suppresses this mode, so this unusual response is a consequence of the constrained setup. A simple estimate shows that this response is energetically feasible. Imagine an equilibrium membrane area $A_0 = 4\pi R_0^2$ is compressed to an area $A = A_0 - \Delta A < A_0$, increasing its stress energy by $\frac{1}{2}K_A(\Delta A)^2/A_0$. It could eliminate the stress by shedding the excess area, but the expelled lipid patch costs a line energy $2\pi r\gamma$, if it is circular with radius $r = \sqrt{\Delta A/\pi}$. Beyond a sufficiently large ΔA this trade-off is beneficial, namely once we satisfy $\frac{\partial}{\partial A}[-\frac{1}{2}K_A(\Delta A)^2/A_0 + 2\pi\gamma\sqrt{\Delta A/\pi}] = 0$, leading to a critical patch radius $r^* = (4\gamma R_0^2/K_A)^{1/3}$. Since for us $\gamma/K_A \approx 0.16\,\sigma \approx 0.13\,$nm, we find that for System IV we get $r^* \approx 5.5\,$nm. As the inset shows, the actual patch is substantially bigger than that, so we are well past that threshold.

This observation shows that instead of lowering the free energy *locally* by pulling out a number of individual chains, the system also has *global* modes available to respond to chain stretching. Since such a collective response can only happen with sufficiently many lipids present, we could not have encountered it in our atomistic simulations. This also vividly illustrates the usefulness of CG simulations for critically evaluating the assumptions that go into theoretical models, which in this case might have missed an important effect: chain pull-out is not the only and indeed need not be the decisive factor bounding NP size from above. Notice that the difference between these two responses has practical implications: the irregular shapes associated with the global scenario might affect the uptake of the NPs,[18,22] hence mechanisms would have to be put into place to avoid them.

Assembly

Having tested the predicted range of stable vesicle sizes using *pre-assembled* nanocomposites, let us now move on to the assembly process. In this section we investigate a *nonequilibrium* formation protocol known as rapid solvent exchange.[32] The idea is to begin with a solvent in which the lipids are well soluble (*e.g.* absolute ethanol), and then rapidly displace it with water, thereby precipitating the lipids into growing bilayers which get anchored onto the tethers. This method is experimentally easy to execute and is routinely used to create sparsely tethered lipid bilayer membranes.[32,35,57] It is also reported to have several advantages compared to other protocols; for instance, the quality of the resulting bilayers, depends much less on the lipid phase state than when the membranes are created by vesicle fusion.[35]

A simplified way to capture this idea in our CG simulations is as follows: begin with an NP core with tethers grafted onto it and randomly add lipids, but first eliminate the tail-tail attraction between lipids which otherwise drives self-assembly (recall that the Cooke[71,72] model is solvent free,

and CG lipids only aggregate due to a cohesive interactions between the tails, which mimic the hydrophobic effect). After a short equilibration time, turn on the tail-cohesion and thereby trigger the formation of bilayers in the bulk as well as onto the tethers of the NP core, as described in more detail in the Methods Section. This system will be referred to as "System V" hereafter.

A sequence of snapshots from this simulation is shown in Figure. 4. Initially, the polymers were grafted to the core and relaxed. Twice as many lipids as in System II were put into a cubic simulation box of side-length $L = 80\sigma \sim 65\,\mathrm{nm}$. Since the lipids still need to assemble into a vesicle around the polymer-coated core, this allows the system to choose its own vesicle radius R_{ves} (Fig. 4a). When the simulation starts, lipids aggregate due to hydrophobic interactions and form some complex and interconnected membrane structures (Fig. 4b). Due to the interaction between the polymers and the vesicle, the excess lipids eventually detached from the membrane enclosing the NP (Fig. 4c, similar to system IV in Fig. 3), leaving a complete coated NP and (in this case) an empty liposome (Fig. 4d).

The assembled nanocomposite has a radius of $r \simeq 13.5\,\mathrm{nm}$, as determined from the radial distribution profile (shown in the Supplementary Information). The resulting radius is within the range predicted by our theoretical model, and in fact quite close to the free energy minimum, $r \simeq 13.2\,\mathrm{nm}$, as shown in Fig. 3. This suggests that a self assembly process can automatically lead to relaxed vesicles, which is not entirely obvious. It would certainly be imaginable that an excess supply of lipids forces more of them into the membrane coat then optimal. Conversely, it would also be conceivable that lipids prefer to form free vesicles over the highly constrained polymer tethered vesicles, thus depriving the coats of lipids. Our simulations suggest that neither is the case, and that the excess vesicles act as a lipid reservoir at sufficiently similar chemical potential to give rise to unstressed membrane coats. The observation that unstressed vesicles with a radius near the expected free energy minimum emerge also confirms that the tethers can indeed pass their uniformity onto the larger level of the whole coated nanoparticle—one of the motivations of our design.

Solvent conditions

Two practical issues showed up in the assembly process described in the previous subsection. The first one is the possibility that a membrane coat with excess lipids may be kinetically trapped in metastable states, even though Fig. 4 shows these excess lipids can detach. In other sets of assembly simulations under very similar conditions we have also observed planar bilayer attachments (similar to the "flap" connected to the vesicle in the right inset of Fig. 3) that stay connected to the coat throughout the entire simulations. The second issue is that empty liposomes (enclosing no core) are also produced from the excess lipids. While their size might be comparable to the NPs, the latter would have a higher density (due to the dense core), and so separating them is no serious difficulty. It would nevertheless be preferable if empty vesicles could be avoided in the first place.

These two issues can be alleviated by a different formation protocol, this time an *equilibrium* one. The basic idea is to *improve* the solvent condition and adjust the lipid concentration to *just below* the critical micelle concentration (CMC). In experiments this is typically done with suitable co-solvents (such as ethanol, methanol, or chloroform), while in our simulation we simply reduce the cohesion strength between all lipid-tail like beads (both for lipids and polymer anchors). Under such conditions, a large amount of lipids stay as monomers or very loose aggregates in the bulk solvent (below CMC), while in the vicinity of the polymer-coated core particle lipids cluster and form a bilayer. The latter is possible because the anchors of the grafted linkers have already lost their entropy, so the entropic penalty to stay together with other lipids is reduced. In other words, the lipids that diffuse to the anchors could stay and lose entropy while still lowering the total free energy of the system by forming a bilayer with the anchors. In this situation, the grafted anchors serve as artificial nucleation sites for the lipids—essentially lowering the local CMC.

We indeed found a range of solvent conditions in which this intriguing phenomenon occurred—bulk lipid solubility but aggregation just around the

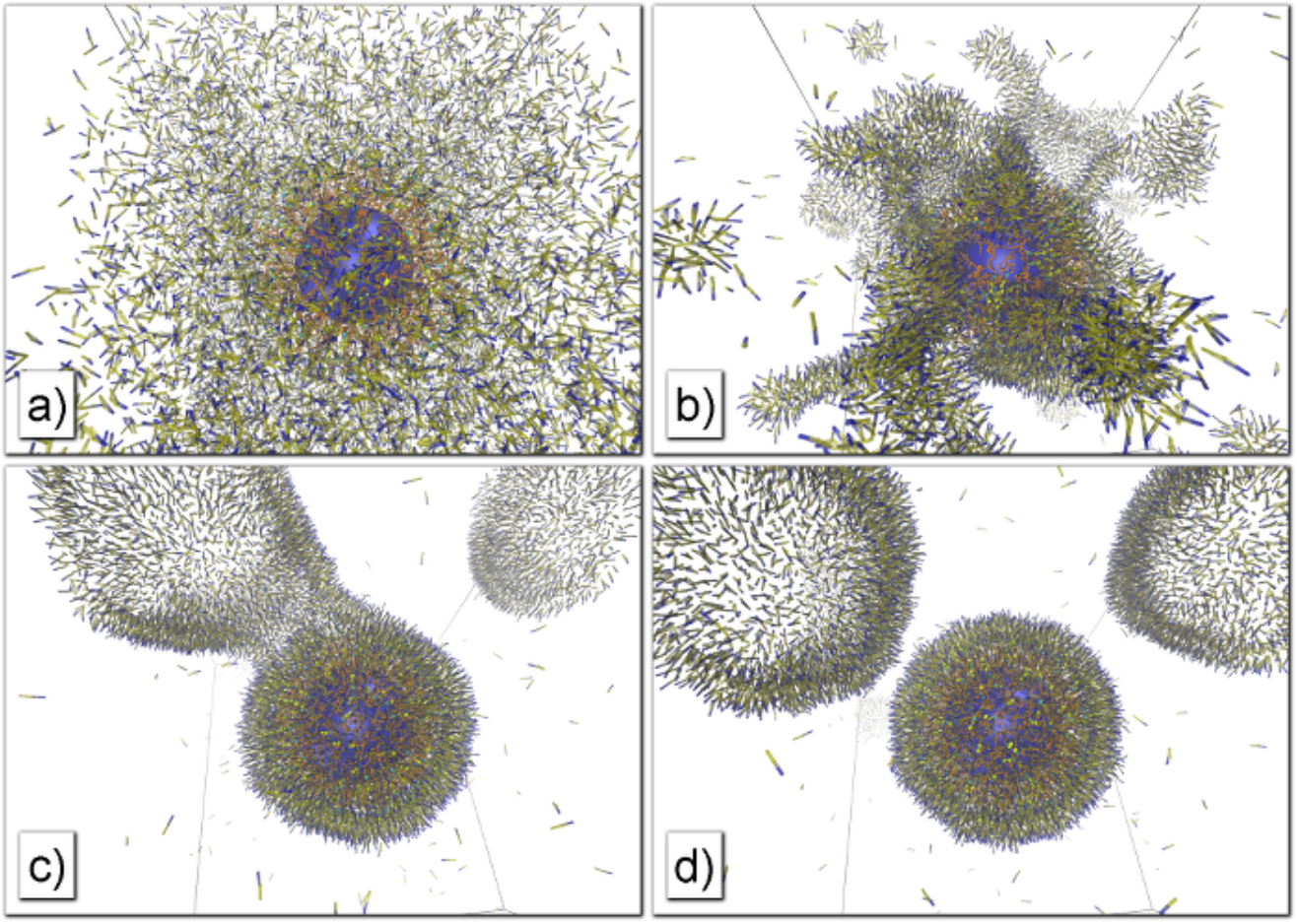

Figure 4: A sequence of snapshots of the assembly of System V. Lipids are rendered as semi-transparent so that the linkers and the core are more visible. (a) initial configuration of grafted polymers and random lipids; (b) lipids start to aggregate into patches; (c) excess lipids are pinching off the NP; (d) final structure of the membrane coated NP.

NPs. For a slightly different system made of 508 linkers on a core of the same size and 10800 lipids in a cubic box of side length $L = 80\,\sigma \sim 65\,\text{nm}$, the configuration after the system has reached equilibrium is shown in Fig. 5. In this case, we needed to decrease the hydrophobic interactions to 55% of their strength under normal aqueous conditions. Given the coarse-grained nature of our system, the important finding is of course not the value of this number but the fact that this scenario of a localized CMC reduction is possible, making it a worthwhile endeavor for experimentalists to search for it and possibly exploit it as an alternative pathway towards assembly of our proposed NPs.

It is also worth noting that these simulations lend further support to our claim that the tethers help stabilize the lipid membrane of our NP construct compared to a bare liposome situation. If the integrity of a bilayer phase surrounding the NP can be enhanced even in a situation in which no bulk membranes are stable, it seems plausible that the lipid anchors at he end of tethers equip the closed bilayer with added stability and self-healing properties also in cases where the bilayer phase is in fact stable but has suffered some localized damaged due to, say, high shear stresses.

Dispersity

In addition to the two potential issues that may be mitigated by adjusting the solvent condition, one may also be concerned about the effect of tether dispersity. Non-uniform chains will also exert non-uniform forces to the lipid vesicle, which could potentially induce local deformations, or prevent the formation of a stable and tight enve-

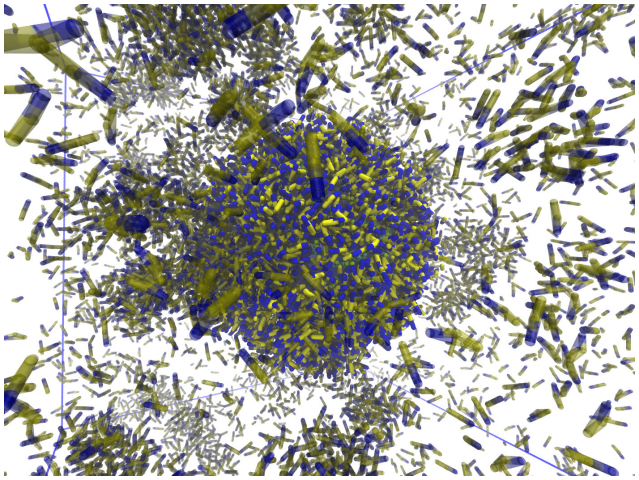

Figure 5: A nanocomposite assembly simulation under different solvent condition. The strength of the attractions among the lipids and anchors was reduced to 55% of its normal level in water. The nanoparticle is covered by 508 linkers with a shorter length of 10 monomers, and the system contains about 10800 lipids. Stray lipids in the bulk are rendered partially transparent, while molecules near the solid core are drawn as normal.

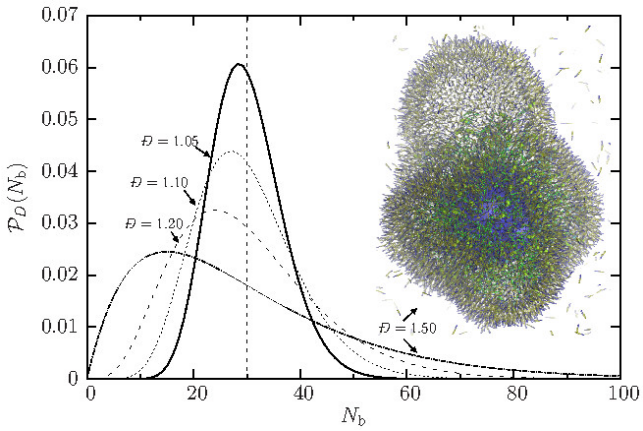

Figure 6: Distribution of chain length for systems with dispersity $Đ \in \{1.05, 1.1, 1.2, 1.5\}$. N_b represents the number of bonds, and $F(N_b)$ is the probability distribution function. All system contain the same number of linkers, and the *average* chain length is 30. For the systems with $Đ = 1.2$ and $Đ = 1.5$ the membrane vesicle has irregular shapes with bulges where no tethers (small orange beads connected to a larger red-blue anchor) are anchored to. For visual clarity, lipids are shown with thin semi-transparent sticks, and the linkers are shown as connected beads.

lope altogether.

Thus, we set up a set of simulations with a dispersity $Đ \in \{1.05, 1.1, 1.2, 1.5\}$ and compare with the uniform System V shown in Fig. 4. The length distribution of the chains was assumed to follow a two-parameter Schulz distribution,[80] with the same 342 linkers and the same average length of 30 monomers per chain. The two parameters were set to reproduce the desired dispersity Đ and the (average) degree of polymerization, namely 30. The probability distribution of chain length is plotted in Fig. 6. The rest of the initial simulation setup was similar to the assembly process with fine-tuned solvent condition in the previous subsection, where the lipids aggregate mainly around the anchored linkers.

Among the four non-uniform systems, only the two lowest dispersities (1.05 and 1.1) successfully formed the desired spherical membrane vesicle around the linkers. In the systems with $Đ = 1.2$ and $Đ = 1.5$ a crumpled bilayer vesicle was observed at the end of the simulations, shown as the inset of Fig. 6. Bulges found in the assembled structure may contain no anchors in the central area, but several long linkers anchored around the rim. Such shapes may be undesired for the uptake of nanocomposites into cells.

Dispersity could be an explanation for the aspherical shape, since chains of various lengths prefer to impose different vesicle radii, thus exerting uneven forces to the membrane. To test whether this observation is not merely a property of our highly coarse-grained model, we also conducted CG simulations on the more refined MARTINI level.[81,82] The MARTINI model follows the procedure outlined in Liu and Faller.[83] Here we use 50 tethers (0.15 tethers/nm^2) of average length 15. This is slightly above the limit beyond which in previous work[83] we have found uniformly tethered membranes to destabilize via buckling. Since the number of PEG-linkers is much smaller than in our full NP simulations, it makes little sense to capture a full Schulz distribution, and hence dispersity was instead modeled by a homogeneous distribution of chains of different lengths, giving the desired dispersity Đ. Specifically, for DJ = 1.22 we use an equimolar mixture of tether lengths 5, 10, 15, 20 and 25. For $Đ = 1.4$ we use 60% tethers of length 15 and 20% each of 10 and 20. Tethers are equally

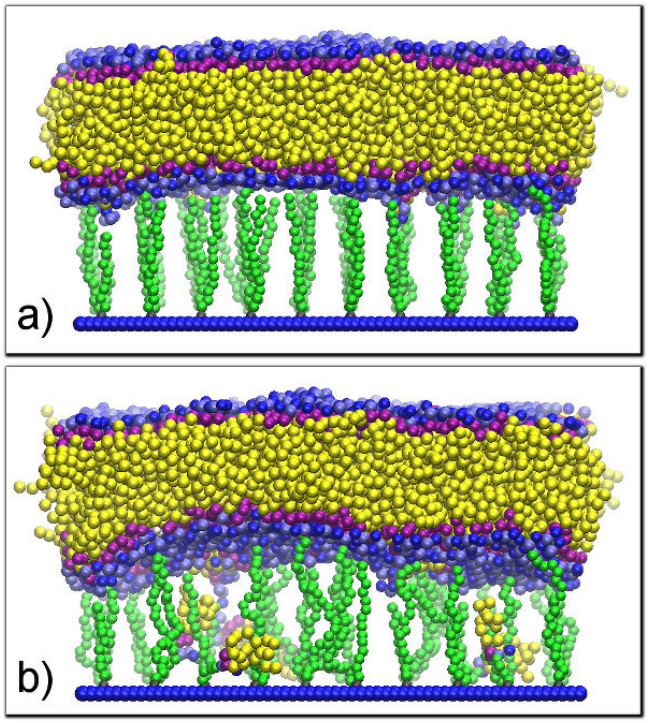

Figure 7: Simulations of tethered bilayers using the MARTINI model (version 1.4). For clarity, water molecules are not shown. The dispersity is (a) Đ = 1.04 and (b) Đ = 1.22. The polymer tethers are marked in green, the phosphocholine headgroup of the lipids is blue, the glycerol backbone is magenta, and the lipid tails are yellow. Notice that for the larger dispersity in panel (b) several of the shorter tethers—and with them the lipid anchors—have pulled out of the bilayer.

spaced, and the different lengths are randomly distributed.

These simulations show that if lipid bilayers are tethered to a flat substrate by means of non-uniform linkers, the proximal leaflet is rougher than the distal one—see Fig. 7. This is in contrast to what is observed in the normal case of uniform anchoring, where the support suppresses fluctuations in the proximal leaflet. A curious implication is that from a fluctuation point of view a membrane tethered by weakly non-uniform linkers is actually *closer* to a free membrane than a uniformly tethered membrane. Compared to our earlier data[83] it actually appears that the weakly non-uniform membranes are more stable than the uniform ones. We would like to emphasize that both sets of simulations use the regular MARTINI model (V 1.4)[84] and not the version with the more

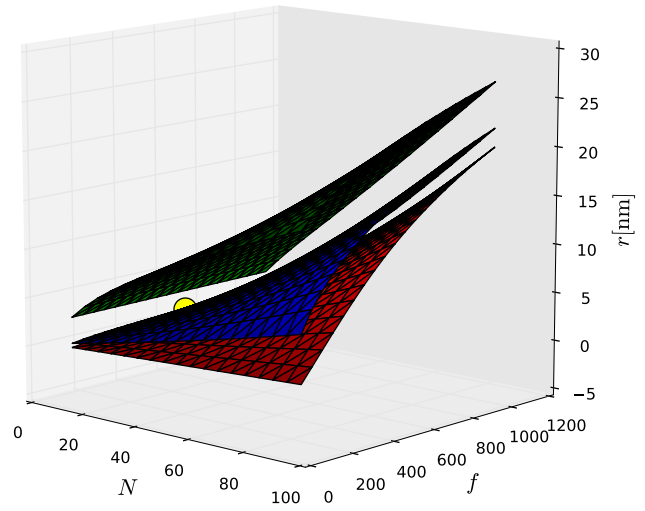

Figure 8: Possible range of the vesicle radius r predicted by our theory. The red, blue, and green surfaces are the minimum $r_{\min}$, relaxed r_0, and maximum $r_{\max}$, respectively, as a function of degree of polymerization N and number of chains f. The range of stable nanocomposites is the subspace between the red and the green surfaces. In this case, a core radius of of $R_{\text{core}} = 9\,\text{nm}$ was chosen. The yellow dot represents the example system studied in Fig. 3.

hydrophobic water,[85] hence the area per lipid is in the experimental range and the membranes are not pre-stressed.

With increasing PDI we also see that short tethers can locally distort or even disrupt the membrane when a tether cannot reach to the average position anymore and it becomes more advantageous to pull out than to disturb the membrane on a larger scale (see red circle in Fig. 7b). Local anchor-pullout is thus seen to compete with global shape distortions. How this plays out in detail likely depends on the realizations of the local tether-length distributions and shall not be pursued further at this point.

Discussion and conclusion

The key objective of this study is to provide guidelines for choosing design parameters and assembly strategies of our proposed nanocomposites, using the theoretical and simulation models described above. We have shown that our theoretical model can fairly accurately predict the compres-

sional state of the polymer brush between core and enclosing bilayer, as compared to simulation, and so we can use our theoretical expressions to explore a wider portion of the interesting parameter space, learning how the choice of various control parameters affects stability and size of NPs.

To illustrate this idea, and following the example systems studied, we fixed the core size $R_{\mathrm{ves}} = 9\,\mathrm{nm}$ as well as the persistence length of the chains $\ell_{\mathrm{p}} \simeq 0.32\,\mathrm{nm}$, but then systematically scan the degree of polymerization, N, and the number of chains, $f = 4\pi R_c^2 \Sigma$, within a reasonably range. Using our theoretical model, we derive three surfaces of minimum radius r_{min}, relaxed radius r_0, and maximum radius r_{max}, as shown in Fig. 8. For orientation, the location of the assembled system V is also labeled in the figure. The possible range of stable nanocomposites is sandwiched in between the r_{min} and r_{max} surface, and optimal stability is achieved at r_0. In cases where, say, f cannot change due to a fixed grafting density Σ and core size R_{core}, the surfaces reduce to three curves within a cross-section with constant f, and one can still pick an optimal N to obtain a desired particle radius. We can see that for all choices of the parameters, the relaxed state is fairly close to the lower bound, while a lot more room is available between there and the upper size. Also, the size of the final nanocomposite can be increased by both N and f, but the impact of the relative changes depends on the value of the other parameter (meaning, the two parameters do not decouple trivially).

Simple theoretical considerations amended by a series of simulations at varying levels of resolution can substantially reduce the parameter space, but the situation remains complex. Especially the kinetic aspects of formation will require more refined studies of the assembly process, likely accounting for the hydrodynamic of solvent mixing. It is still our hope that our investigation helps to narrow down experiential conditions enough to make systematic synthesis and assembly studies feasible, thus helping to create NP constructs with a wide variety of highly promising properties.

Methods Section

Coarse-grained model of tethered lipid systems

Due to the size and the complexity of our NP system, a coarse-grained (CG) simulation model, in which a group of several atoms is represented by one CG bead, is necessary in order to reach the long time scale required, for instance, by the assembly process.

For the phospholipids, we adopted the well-tested model by Cooke *et al.*,[71,72] in which each lipid consists of a chain of 3 CG beads, one for the headgroup and two consecutive ones for the tails. With no solvent molecules in the model, the hydrophobic interaction is represented by a long-ranged attraction among the hydrophobic tail beads. We chose the attraction range $w_{\mathrm{c}} = 1.72\sigma$ in order to produce an lipid aspect ratio similar to DOPC (1,2-dioleoyl-sn-glycero-3-phosphocholine), giving a bending modulus of $20 - 25 k_{\mathrm{B}}T$ at body temperature.

With the aspect ratio matched, the length scales in this CG membrane can be mapped to a real DOPC membrane, giving a conversion factor of $1\,\mathrm{nm} = 1.236\,\sigma$, where σ is the length unit in simulations. The thermal energy $k_{\mathrm{B}}T = 1.1\varepsilon$ in simulations can also be translated to real units by using the value of $k_{\mathrm{B}}T$. Assuming body temperature, we get $1\varepsilon = k_{\mathrm{B}}T/1.1 \approx 4.3\,\mathrm{pN}\cdot\mathrm{nm}/1.1 = 3.9\,\mathrm{pN}\cdot\mathrm{nm}$.

For the linker molecules, the Cooke model was extended by conjugating a soft hydrophilic polymer to the headgroup of the lipids, using the same functional forms for the interactions. The beads composing the polymers are chosen half as big as the ones in the lipids and the bonded interactions have been parameterized to give a persistence length comparable to that of PEG. The open ends of the chains were fixed to the NP core in simulations.

Rapid Solvent Exchange

The rapid solvent exchange process is implemented in the following way: first, the tether molecules were grafted to the surface of the core in the same way as we measured the force-extension relation of the brush; second, lipids with ran-

dom positions and orientations were added into the simulation box, analogous to lipids in good organic solvents; third, the hydrophobic interactions among the lipids, which drives their self-assembly process, were turned on, similar to the case in aqueous solution.

Compared to real rapid solvent exchange, the onset of aggregation of the lipids in simulations happens on a much short time scale. We could have gradually tuned up the strength of these interactions to represent the real process better. However, this is unlikely to affect the equilibrium configurations. Thus, we chose to adopt this simpler version for the sake of computational efficiency. What might be more troublesome is that the actual mixing process, during which water is rapidly added to a good solvent for the lipids, is not actually accounted for. A more realistic implementation of the rapid solvent exchange process would require some treatment of hydrodynamics, but this is beyond the scope of this simple model.

Acknowledgement The authors thank Richard Gandour, Alan Esker, and Mathias Lösche for helpful discussions. NSF CDI grant #0941690 is gratefully acknowledged.

Supporting Information Available: Details about the spherical polymer brush theory, our CG model, and simulation setups can be found in the Supporting Information. This material is available free of charge via the Internet at `http://pubs.acs.org/`.

References

1. Allen, T. M.; Cullis, P. R. Drug Delivery Systems: Entering the Mainstream. *Science* **2004**, *303*, 1818 –1822.

2. Peer, D.; Karp, J. M.; Hong, S.; Farokhzad, O. C.; Margalit, R.; Langer, R. Nanocarriers as an emerging platform for cancer therapy. *Nature Nanotechnol.* **2007**, *2*, 751–760.

3. Davis, M. E.; Chen, Z. G.; Shin, D. M. Nanoparticle therapeutics: an emerging treatment modality for cancer. *Nature Rev. Drug Discovery* **2008**, *7*, 771–782.

4. Brannon-Peppas, L.; Blanchette, J. O. Nanoparticle and targeted systems for cancer therapy. *Adv. Drug Delivery Rev.* **2012**, *64*, 206–212.

5. Mudshinge, S. R.; Deore, A. B.; Patil, S.; Bhalgat, C. M. Nanoparticles: emerging carriers for drug delivery. *Saudi Pharm. J.* **2011**, *19*, 129–141.

6. Bamrungsap, S.; Zhao, Z.; Chen, T.; Wang, L.; Li, C.; Fu, T.; Tan, W. Nanotechnology in therapeutics: a focus on nanoparticles as a drug delivery system. *Nanomedicine (UK)* **2012**, *7*, 1253–1271.

7. Parveen, S.; Misra, R.; Sahoo, S. K. Nanoparticles: a boon to drug delivery, therapeutics, diagnostics and imaging. *Nanomed.–Nanotechnol.* **2012**, *8*, 147–166.

8. Doane, T. L.; Burda, C. The unique role of nanoparticles in nanomedicine: imaging, drug delivery and therapy. *Chem. Soc. Rev.* **2012**, *41*, 2885–2911.

9. Cavadas, M.; González-Fernández, A.; Franco, R. Pathogen-mimetic stealth nanocarriers for drug delivery: a future possibility. *Nanomed.–Nanotechnol.* **2011**, *7*, 730–743.

10. Allen, T. M.; Cullis, P. R. Liposomal drug delivery systems: From concept to clinical applications. *Adv. Drug Deliver. Rev.* **2013**, *65*, 36–48.

11. DeSimone, J. M.; Petros, R. A. Strategies in the design of nanoparticles for therapeutic applications. *Nature Rev. Drug Discov.* **2010**, *9*, 615–627.

12. Scheinberg, D. A.; Villa, C. H.; Escorcia, F. E.; McDevitt, M. R. Conscripts of the infinite armada: systemic cancer therapy using nanomaterials. *Nature Rev. Clin. Oncol.* **2010**, *7*, 266–276.

13. Kwon, I. K.; Lee, S. C.; Han, B.; Park, K. Analysis on the current status of targeted drug delivery to tumors. *J. Control. Release* **2012**, *164*, 108–114.

14. Ganta, S.; Devalapally, H.; Shahiwala, A.; Amiji, M. A review of stimuli-responsive nanocarriers for drug and gene delivery. *J. Control. Release* **2008**, *126*, 187–204.

15. Barenholz, Y. C. Doxil®—the first FDA-approved nano-drug: lessons learned. *J. Control. Release* **2012**, *160*, 117–134.

16. Janib, S. M.; Moses, A. S.; MacKay, J. A. Imaging and drug delivery using theranostic nanoparticles. *Adv. Drug. Deliv. Rev.* **2010**, *62*, 1052–1063.

17. Florence, A. T. "Targeting" nanoparticles: The constraints of physical laws and physical barriers. *J. Control. Release* **2012**, *164*, 115–124.

18. Albanese, A.; Tang, P. S.; Chan, W. C. W. The Effect of Nanoparticle Size, Shape, and Surface Chemistry on Biological Systems. *Annu. Rev. Biomed. Eng.* **2012**, *14*, 1–16.

19. Moghimi, S. M.; Hunter, A. C.; Andresen, T. L. Factors Controlling Nanoparticle Pharmacokinetics: An Integrated Analysis and Perspective. *Ann. Rev. Pharmacol. Toxicol.* **2012**, *52*, 481–503.

20. De Jong, W. H.; Hagens, W. I.; Krystek, P.; Burger, M. C.; Sips, A. J.; Geertsma, R. E. Particle size-dependent organ distribution of gold nanoparticles after intravenous administration. *Biomaterials* **2008**, *29*, 1912–1919.

21. Tzlil, S.; Deserno, M.; Gelbart, W. M.; Ben-Shaul, A. A Statistical-Thermodynamic Model of Viral Budding. *Biophys. J.* **2004**, *86*, 2037–2048.

22. Chithrani, B. D.; Ghazani, A. A.; Chan, W. C. W. Determining the Size and Shape Dependence of Gold Nanoparticle Uptake into Mammalian Cells. *Nano Letters* **2006**, *6*, 662–668.

23. Zhang, S.; Li, J.; Lykotrafitis, G.; Bao, G.; Suresh, S. Size-Dependent Endocytosis of Nanoparticles. *Adv. Mater.* **2009**, *21*, 419–424.

24. Ferrari, M. Nanogeometry: Beyond drug delivery. *Nature Nanotechnol.* **2008**, *3*, 131–2.

25. Vockenroth, I. K.; Ohm, C.; Robertson, J. W. F.; McGillivray, D. J.; Lösche, M.; Köper, I. Stable insulating tethered bilayer lipid membranes. *Biointerphases* **2008**, *3*, FA68–FA73.

26. Xie, J.; Lee, S.; Chen, X. Nanoparticle-based theranostic agents. *Adv. Drug. Deliv. Rev.* **2010**, *62*, 1064–1079.

27. Lammers, T.; Aime, S.; Hennink, W. E.; Storm, G.; Kiessling, F. Theranostic Nanomedicine. *Accounts Chem. Res.* **2011**, *44*, 1029–1038.

28. Choi, K. Y.; Liu, G.; Lee, S.; Chen, X. Theranostic nanoplatforms for simultaneous cancer imaging and therapy: current approaches and future perspectives. *Nanoscale* **2012**, *4*, 330–342.

29. Mieszawska, A. J.; Mulder, W. J. M.; Fayad, Z. A.; Cormode, D. P. Multifunctional Gold Nanoparticles for Diagnosis and Therapy of Disease. *Mol. Pharm.* **2013**, *10*, 831–847.

30. Bangham, A. D.; Standish, M. M.; Watkins, J. C. Diffusion of univalent ions across the lamellae of swollen phospholipids. *J. Mol. Biol.* **1965**, *13*, 238–252.

31. Torchilin, V. P. Recent advances with liposomes as pharmaceutical carriers. *Nature Rev. Drug Discov.* **2005**, *4*, 145–160.

32. Cornell, B. A.; Braach-Maksvytis, V. L. B.; King, L. G.; Osman, P. D. J.; Raguse, B.; Wieczorek, L.; Pace, R. J. A biosensor that uses ion-channel switches. *Nature* **1997**, *387*, 580–583.

33. Raguse, B.; Braach-Maksvytis, V.; Cornell, B. A.; King, L. G.; Osman, P. D. J.; Pace, R. J.; Wieczorek, L. Tethered Lipid Bilayer Membranes: Formation and Ionic Reservoir Characterization. *Langmuir* **1998**, *14*, 648–659.

34. Wagner, M.; Tamm, L. Tethered Polymer-Supported Planar Lipid Bilayers for Reconstitution of Integral Membrane Proteins: Silane-Polyethyleneglycol-Lipid as a Cushion and Covalent Linker. *Biophys. J.* **2000**, *79*, 1400–1414.

35. McGillivray, D. J.; Valincius, G.; Vanderah, D. J.; Febo-Ayala, W.; Woodward, J. T.; Heinrich, F.; Kasianowicz, J. J.; LöÃűsche, M. Molecular-scale structural and functional characterization of sparsely tethered bilayer lipid membranes. *Biointerphases* **2007**, *2*, 21–33.

36. Mandal, B.; Bhattacharjee, H.; Mittal, N.; Sah, H.; Balabathula, P.; Thoma, L. A.; Wood, G. C. Core–shell-type lipid–polymer hybrid nanoparticles as a drug delivery platform. *Nanomed.–Nanotechnol.* **2013**, *9*, 474–491.

37. Saleh, N.; Sarbu, T.; Sirk, K.; Lowry, G. V.; Matyjaszewski, K.; Tilton, R. D. Oil-in-water emulsions stabilized by highly charged polyelectrolyte-grafted silica nanoparticles. *Langmuir* **2005**, *21*, 9873–9878.

38. Saleh, N.; Phenrat, T.; Sirk, K.; Dufour, B.; Ok, J.; Sarbu, T.; Matyjaszewski, K.; Tilton, R. D.; Lowry, G. V. Adsorbed triblock copolymers deliver reactive iron nanoparticles to the oil/water interface. *Nano Lett.* **2005**, *5*, 2489–2494.

39. Alivisatos, A. P.; Johnsson, K. P.; Peng, X.; Wilson, T. E.; Loweth, C. J.; Bruchez, M. P.; Schultz, P. G. Organization of 'nanocrystal molecules' using DNA. *Nature* **1996**, *382*, 609–611.

40. Mirkin, C. A.; Letsinger, R. L.; Mucic, R. C.; Storhoff, J. J. A DNA-based method for rationally assembling nanoparticles into macroscopic materials. *Nature* **1996**, *382*, 607–609.

41. Park, S. Y.; Lytton-Jean, A. K. R.; Lee, B.; Weigand, S.; Schatz, G. C.; Mirkin, C. A. DNA-programmable nanoparticle crystallization. *Nature* **2008**, *451*, 553–556.

42. Schiffelers, R. M.; Ansari, A.; Xu, J.; Zhou, Q.; Tang, Q.; Storm, G.; Molema, G.; Lu, P. Y.; Scaria, P. V.; Woodle, M. C. Cancer siRNA therapy by tumor selective delivery with ligand-targeted sterically stabilized nanoparticle. *Nucleic Acids Res.* **2004**, *32*, e149–e149.

43. Rosi, N. L.; Giljohann, D. A.; Thaxton, C. S.; Lytton-Jean, A. K. R.; Han, M. S.; Mirkin, C. A. Oligonucleotide-modified gold nanoparticles for intracellular gene regulation. *Science* **2006**, *312*, 1027–1030.

44. Elghanian, R.; Storhoff, J. J.; Mucic, R. C.; Letsinger, R. L.; Mirkin, C. A. Selective colorimetric detection of polynucleotides based on the distance-dependent optical properties of gold nanoparticles. *Science* **1997**, *277*, 1078–1081.

45. Taton, T. A.; Mirkin, C. A.; Letsinger, R. L. Scanometric DNA array detection with nanoparticle probes. *Science* **2000**, *289*, 1757–1760.

46. Gao, X.; Cui, Y.; Levenson, R. M.; Chung, L. W. K.; Nie, S. In vivo cancer targeting and imaging with semiconductor quantum dots. *Nature Biotech.* **2004**, *22*, 969–976.

47. Cheng, J.; Teply, B. A.; Sherifi, I.; Sung, J.; Luther, G.; Gu, F. X.; Levy-Nissenbaum, E.; Radovic-Moreno, A. F.; Langer, R.; Farokhzad, O. C. Formulation of functionalized PLGA–PEG nanoparticles for in vivo targeted drug delivery. *Biomaterials* **2007**, *28*, 869–876.

48. Von Werne, T.; Patten, T. E. Preparation of structurally well-defined polymer-nanoparticle hybrids with controlled/living radical polymerizations. *J. Am. Chem. Soc.* **1999**, *121*, 7409–7410.

49. Perruchot, C.; Khan, M. A.; Kamitsi, A.; Armes, S.; von Werne, T.; Patten, T. E. Synthesis of well-defined, polymer-grafted silica particles by aqueous ATRP. *Langmuir* **2001**, *17*, 4479–4481.

50. Allen, T. M.; Brandeis, E.; Hansen, C. B.; Kao, G. Y.; Zalipsky, S. A new strategy for attachment of antibodies to sterically stabilized liposomes resulting in efficient targeting to cancer cells. *BBA–Biomembranes* **1995**, *1237*, 99–108.

51. Torchilin, V. P. Drug targeting. *Eur. J. Pharm. Sci.* **2000**, *11*, S81–S91.

52. Siepmann, J.; Peppas, N. A. Modeling of drug release from delivery systems based on hydroxypropyl methylcellulose (HPMC). *Adv. Drug. Deliv. Rev.* **2001**, *48*, 139–157.

53. Peppas, N. A. Historical perspective on advanced drug delivery: How engineering design and mathematical modeling helped the field mature. *Adv. Drug Deliv. Rev.* **2013**, *65*, 5–9.

54. Michor, F.; Liphardt, J.; Ferrari, M.; Widom, J. What does physics have to do with cancer? *Nature Rev. Cancer* **2011**, *11*, 657–670.

55. Ding, H.-M.; Tian, W.-D.; Ma, Y.-Q. Designing Nanoparticle Translocation through Membranes by Computer Simulations. *ACS Nano* **2012**, *6*, 1230–1238.

56. Huynh, L.; Neale, C.; Pomès, R.; Allen, C. Computational approaches to the rational design of nanoemulsions, polymeric micelles, and dendrimers for drug delivery. *Nanomed.–Nanotechnol.* **2012**, *8*, 20–36.

57. Heinrich, F.; Ng, T.; Vanderah, D. J.; Shekhar, P.; Mihailescu, M.; Nanda, H.; Lösche, M. A New Lipid Anchor for Sparsely Tethered Bilayer Lipid Membranes. *Langmuir* **2009**, *25*, 4219–4229.

58. Helfrich, W. The size of bilayer vesicles generated by sonication. *Phys. Lett. A* **1974**, *50*, 115–116.

59. Fromherz, P. Lipid-vesicle structure: Size control by edge-active agents. *Chem. Pjhys. Lett.* **1983**, *94*, 259–266.

60. Hu, M.; Briguglio, J. J.; Deserno, M. Determining the Gaussian Curvature Modulus of Lipid Membranes in Simulations. *Biophys. J.* **2012**, *102*, 1403–1410.

61. Helfrich, W. Elastic properties of lipid bilayers: theory and possible experiments. *Z. Naturforsch. C* **1973**, *28*, 693–703.

62. de Gennes, P.-G. *Scaling concepts in polymer physics*; Cornell University Press: Ithaca, N.Y., 1979.

63. de Gennes, P. G. Conformations of Polymers Attached to an Interface. *Macromolecules* **1980**, *13*, 1069–1075.

64. de Gennes, P. G. Polymers at an interface; a simplified view. *Adv. Colloid Interface Sci.* **1987**, *27*, 189–209.

65. Israelachvili, J. N. *Intermolecular and surface forces*, 2nd ed.; Academic Press London,, 1991.

66. Hu, M. Designing polymer-tethered membrane-nanoparticle composites. Ph.D. thesis, Carnegie Mellon University, 2013.

67. Rosa, A.; Hoang, T. X.; Marenduzzo, D.; Maritan, A. Elasticity of Semiflexible Polymers with and without Self-Interactions. *Macromolecules* **2003**, *36*, 10095–10102.

68. Cifra, P.; Bleha, T. Stretching of self-interacting wormlike macromolecules. *Polymer* **2007**, *48*, 2444–2452.

69. Marko, J. F.; Siggia, E. D. Stretching DNA. *Macromolecules* **1995**, *28*, 8759–8770.

70. Tanford, C. *The Hydrophobic Effect*, 2nd ed.; Wiley: New York, 1980.

71. Cooke, I. R.; Kremer, K.; Deserno, M. Tunable generic model for fluid bilayer membranes. *Phys. Rev. E* **2005**, *72*, 011506.

72. Cooke, I. R.; Deserno, M. Solvent-free model for self-assembling fluid bilayer membranes: Stabilization of the fluid phase based on broad attractive tail potentials. *J. Chem. Phys.* **2005**, *123*, 224710.

73. Harmandaris, V. A.; Deserno, M. A novel method for measuring the bending rigidity of model lipid membranes by simulating tethers. *J. Chem. Phys.* **2006**, *125*, 204905.

74. Hu, M.; Diggins, P.; Deserno, M. Determining the bending modulus of a lipid membrane by simulating buckling. *J. Chem. Phys.* **2013**, *138*, 214110–214110–13.

75. Cooke, I. R.; Deserno, M. Coupling between Lipid Shape and Membrane Curvature. *Biophys. J.* **2006**, *91*, 487–495.

76. Illya, G.; Deserno, M. Coarse-Grained Simulation Studies of Peptide-Induced Pore Formation. *Biophys. J.* **2008**, *95*, 4163–4173.

77. Reynwar, B. J.; Illya, G.; Harmandaris, V. A.; Müller, M. M.; Kremer, K.; Deserno, M. Aggregation and vesiculation of membrane proteins by curvature-mediated interactions. *Nature* **2007**, *447*, 461–464.

78. Hoopes, M. I.; Deserno, M.; Longo, M. L.; Faller, R. Coarse-grained modeling of interactions of lipid bilayers with supports. *J. Chem. Phys.* **2008**, *129*, 175102.

79. Grest, G. S.; Kremer, K. Molecular dynamics simulation for polymers in the presence of a heat bath. *Phys. Rev. A* **1986**, *33*, 3628–3631.

80. Rogošić, M.; Mencer, H.; Gomzi, Z. Polydispersity index and molecular weight distributions of polymers. *Eur. Polym. J.* **1996**, *32*, 1337–1344.

81. Marrink, S. J.; Risselada, H. J.; Yefimov, S.; Tieleman, D. P.; de Vries, A. H. The MARTINI Force Field: Coarse Grained Model for Biomolecular Simulations. *J. Phys. Chem. B* **2007**, *111*, 7812–7824.

82. Marrink, S. J.; Tieleman, D. P. Perspective on the MARTINI model. *Chem. Soc. Rev.* **2013**, *42*, 6801–6822.

83. Liu, C.; Faller, R. Conformational, Dynamical. and Tensional Study of Tethered Bilayer Lipid Membranes in Coarse-Grained Molecular Simulations. *Langmuir* **2012**, *28*, 15907–15915.

84. Marrink, S. J.; de Vries, A. H.; Mark, A. E. Coarse Grained Model for Semiquantitative Lipid Simulations. *J. Phys. Chem. B* **2004**, *108*, 750–760.

85. Xing, C.; Faller, R. Interactions of Lipid Bilayers with Supports: A Coarse-Grained Molecular Simulation Study. *J. Phys. Chem. B* **2008**, *112*, 7086–7094.

Graphical TOC Entry